J Mater Sci: Mater Electron (2017) 28:4763–4771
DOI 10.1007/s10854-016-6121-x

$Ba_{0.06}(Na_{1/2}Bi_{1/2})_{0.94}TiO_3$–$Ba(Fe_{1/2}Ta_{1/2})O_3$: giant permittivity lead-free ceramics

Sumit K. Roy[1] · S. N. Singh[2] · S. K. Mukherjee[3] · K. Prasad[4,5]

Received: 8 October 2016 / Accepted: 19 November 2016 / Published online: 29 November 2016

Abstract Perovskite type lead-free $(1-x)Ba_{0.06}(Na_{1/2}Bi_{1/2})_{0.94}TiO_3$–$xBa(Fe_{1/2}Ta_{1/2})O_3$ $(0 \leq x \leq 1.0)$ ceramics have been synthesized using solid-state reaction method and characterized by X-ray diffraction, scanning electron microscopy, FTIR, Raman spectroscopy and dielectric studies. X-ray diffraction studies of all the ceramics suggested the formation of single phase with crystal structure transforming from rhombohedral–tetragonal ($R3c$) to hexagonal ($P3m1$) symmetry with the increase in $Ba(Fe_{1/2}Ta_{1/2})O_3$-content. Raman and FTIR spectra also confirmed the formation of single phase solid solutions. Dielectric studies showed the giant permittivity $\sim 10^6$ in $x = 0.50$ and 0.75 compositions and the phase transition is found to be of diffusive character. The simultaneous occurrence of compositional fluctuations and weak ferroelectric interactions were considered to be the main cause for diffusivity.

✉ K. Prasad
k.prasad65@gmail.com

[1] Department of Physics, St. Xavier's College, Ranchi 834 001, India

[2] University Department of Physics, Ranchi University, Ranchi 834 008, India

[3] Department of Physics, BIT, Mesra, Ranchi 835 215, India

[4] Aryabhatta Centre for Nanoscience and Nanotechnology, Aryabhatta Knowledge University, Patna 800 001, India

[5] Present Address: University Department of Physics, T.M. Bhagalpur University, Bhagalpur 812 007, India

1 Introduction

The growing demands to develop lead-free materials with very high dielectric constant in the fields of electronics, power plants, aerospace, aeronautic and automotive industries have received considerable attention nowadays. In recent years, complex perovskites with nominal chemical formula $A(Fe_{1/2}B_{1/2})O_3$ ($A \equiv$ Ba, Sr, and Ca; $B \equiv$ Nb, Ta and Sb) have attracted much attention because of their giant dielectric (10^3–10^5) response over a wide temperature and frequency interval [1–5]. $Ba(Fe_{1/2}Ta_{1/2})O_3$ (BFT), in particular, is considered to be one of the interesting materials among them. Galasso et al. [6] reported that BFT has a cubic perovskite structure and shows ferroelectric properties and the cubic structure of BFT, at room temperature, was confirmed in another report too [7]. Further, Agranovskaya [8] found an ambiguous dielectric characteristic of BFT with a large dielectric loss tangent (more than 1). Later on, Filip'ev et al. [9] also found that BFT had a cubic symmetry which cannot possess ferroelectric properties. It was understood that, even though the B-site of BFT is disordered, it does not reveal a ferroelectric DPT phenomena due to the cubic crystal symmetry [9, 10]. Furthermore, Li et al. [11] examined the Mössbauer spectra and carried the TEM study of BFT and suggested that the true symmetry of BFT is trigonal with space group $P3m1$. Also, they studied the pseudo-binary $BaTiO_3$–$Ba(Fe_{1/2}Ta_{1/2})O_3$ system and reported that the dielectric peaks are not frequency dependent and dielectric constant maximum shifts towards lower temperature side with the increase of Fe/Ta content. In a recent work, it was demonstrated that Al_2O_3 doping can effectively improve the dielectric characteristics of BFT [12]. Phatungthane et al. [13] extensively investigated $Ba(Fe_{1/2}Ta_{1/2})O_3$–$Ba(Zn_{1/3}Ta_{2/3})O_3$ ceramics for resonator applications.

Recently, highly pure green light emission has been observed in perovskite $CsPbBr_3$ based light emitting diode [14, 15]. Besides, available literatures suggested that Bi-based compounds are one of the most likely replacements to the lead-based materials due to environmental concern [16, 17]. Among the Bi-based systems, $(1-x)(Bi_{1/2}Na_{1/2})TiO_3$–$xBaTiO_3$ is considered to be one of the potential non-lead candidates for dielectric and/or piezoelectric applications. It exhibits a rhombohedral–tetragonal morphotropic phase boundary (MPB) around $0.06 \leq x \leq 0.08$ with remarkable dielectric, piezoelectric and electromagnetic properties [18, 19]. However, no report to the best of authors' knowledge, has so far been prospected on the non-lead pseudo-binary solid-solution of $Ba_{0.06}(Na_{1/2}Bi_{1/2})_{0.94}TiO_3$–$Ba(Fe_{1/2}Ta_{1/2})O_3$ and this fact is the crux of motivation of this research.

As both $Ba_{0.06}(Na_{1/2}Bi_{1/2})_{0.94}TiO_3$ and $Ba(Fe_{1/2}Ta_{1/2})O_3$ are typical perovskite-type compounds and could be expected to form solid solutions. The elements present at A-site in undoped $Ba_{0.06}(Bi_{1/2}Na_{1/2})_{0.94}TiO_3$ (BNBT) have ionic radii $r\left(Ba^{2+}_{XII}\right) = 1.61$ Å, $r\left(Na^{2+}_{XII}\right) = 1.03$ Å and $r\left(Bi^{3+}_{VIII}\right) = 1.39$ Å [20], here the subscript represents the coordination number. The average ionic radius of A-site is $\langle r_A \rangle = 1.234$ Å. The ionic radius of B-site is $\langle r_B \rangle = r\left(Ti^{4+}_{VI}\right) = 0.605$ Å. Transition metal Fe and Ta in $Ba(Fe_{1/2}Ta_{1/2})O_3$ has ionic radius $r\left(Fe^{3+}_{VI}\right) = 0.645$ Å and $r\left(Ta^{5+}_{VI}\right) = 0.69$ Å. The involved degree of ionic radius mismatch for Fe/Ta substituting the A-site cation or B-site cation will be $\Delta r_A = \left|\langle r_A \rangle - r\left(Fe^{3+}_{VI}\right)\right| = 0.589$ Å or $\left|\langle r_A \rangle - r\left(Ta^{5+}_{VI}\right)\right| = 0.544$ Å and $\Delta r_B = \left|\langle r_B \rangle - r\left(Fe^{3+}_{VI}\right)\right| = 0.04$ Å or $\left|\langle r_B \rangle - r\left(Ta^{5+}_{VI}\right)\right| = 0.085$ Å. Thus Fe^{3+}_{VI} or Ta^{5+}_{VI} are more likely to be incorporated into the B site of BNBT matrix. Inclusion of Fe/Ta into B site also ensures less stress as compared to that into A-site. To understand the structure of the material and comparison of similar ions on the same site Goldschmidt tolerance factor [21] is considered as a useful tool in determining the correct trends, when used with proper coordination numbers. Considering the tolerance factor, the coulombic and strain interactions, and the charge balance, the possible B-site substitution for the solid solution of $Ba_{0.06}(Na_{1/2}Bi_{1/2})_{0.94}TiO_3$ and $Ba(Fe_{1/2}Ta_{1/2})O_3$ could be formulated as $Ba_{0.06+0.94x}Na_{0.47(1-x)}Bi_{0.47(1-x)}Fe_{0.5x}Ta_{0.5x}Ti_{(1-x)}O_3$. Therefore, it is of interest to study the structural and electrical properties of $Ba_{0.06}(Na_{1/2}Bi_{1/2})_{0.94}TiO_3$–$Ba(Fe_{1/2}Ta_{1/2})O_3$ ceramic system. Accordingly, present work reports the effects of BFT addition on the structural and dielectric properties of BNBT ceramics. To this end, $(1-x)$BNBT–xBFT ($0 \leq x \leq 1.0$) powders were synthesized using standard solid-state reaction method and the X-ray diffraction, scanning electron microscopy, FTIR and Raman spectroscopy and dielectric studies were carried out.

2 Experimental

The polycrystalline samples $Ba_{0.06}(Na_{1/2}Bi_{1/2})_{0.94}TiO_3$ (BNBT) and $Ba(Fe_{1/2}Ta_{1/2})O_3$ (BFT) were prepared separately by solid-state reaction technique using high purity (>99.9%) carbonates/oxides of $BaCO_3$, Na_2CO_3, Bi_2O_3, TiO_2 and Ta_2O_5. Following thermochemical reactions were carried out in air atmosphere at 1140 and 1325 °C respectively. $0.06BaCO_3 + \frac{0.94}{4}Na_2CO_3 + \frac{0.94}{4}Bi_2O_3 + TiO_2 \xrightarrow{\Delta} Ba_{0.06}(Na_{1/2}Bi_{1/2})_{0.94}TiO_3 + 0.295CO_2(g)\uparrow$ and $BaCO_3 + \frac{1}{4}Fe_2O_3 + \frac{1}{4}Ta_2O_5 \xrightarrow{\Delta} Ba(Fe_{1/2}Ta_{1/2})O_3 + CO_2(g)\uparrow$. Completion of reaction and the formation of desired compounds were checked by X-ray diffraction technique. BNBT was then doped with varying percentages of BFT. Wet mixing was carried out with methanol as the medium for homogeneous mixing. A series of $(1-x)Ba_{0.06}(Na_{1/2}Bi_{1/2})_{0.94}TiO_3$–$xBa(Fe_{1/2}Ta_{1/2})O_3$ ($x = 0$, 0.10, 0.25, 0.50, 0.75, 0.90 and 1.0) samples were compacted into thin ($\sim$1.5 mm) cylindrical disks with an applied uniaxial pressure 5 Tons. The samples were finally sintered between 1180 and 1350 °C for 4 h. The sintered pellets were ground carefully to ensure the parallel surfaces. The circular surfaces of the disks were covered with thin silver paste layers and fired at 500 °C for 30 min, which act as the electrodes for the electrical measurements. The XRD spectra were recorded using sintered pellet of $(1-x)Ba_{0.06}(Na_{1/2}Bi_{1/2})_{0.94}TiO_3$–$xBa(Fe_{1/2}Ta_{1/2})O_3$ ($0 \leq x \leq 1.0$) with an X-ray diffractometer (XPERT-PRO, Pan Analytical) at room temperature, using CuKα radiation ($\lambda = 1.5406$ Å), over a wide range of Bragg angles ($10° \leq 2\theta \leq 80°$).

The microstructure of all the specimens was obtained by a scanning electron microscopy (SEM Hitachi S-3400N, Japan) on the fractured surface. The Fourier Transformed Infrared (FTIR) spectra of $(1-x)Ba_{0.06}(Na_{1/2}Bi_{1/2})_{0.94}TiO_3$–$xBa(Fe_{1/2}Ta_{1/2})O_3$ ($0 \leq x \leq 1.0$) samples were collected in the transmission mode using an Alpha-T Bruker FTIR spectrophotometer in the range of 500–4000 cm^{-1}. The Raman spectra were obtained using a single monochromator micro-Raman spectrometer (Renishaw inVia Raman Microscope) and excitation wavelengths were provided by a diode laser with an exciting wavelength of 785 nm. The sintered pellets were polished and electroded with air-drying silver paste (SPI supplier, USA) to measure the electrical properties. Dielectric measurements were carried out using a computer-interfaced Impedance analyzer

(E4990A-120, Keysight Technologies, USA). The temperature was varied at a rate of 5 °C/min.

3 Results and discussion

With an aim to study the effect of $Ba(Fe_{1/2}Ta_{1/2})O_3$ addition to $Ba_{0.06}(Na_{1/2}Bi_{1/2})_{0.94}TiO_3$ on the unit cell structure, Rietveld analysis of $(1-x)Ba_{0.06}(Na_{1/2}Bi_{1/2})_{0.94}TiO_3$–$xBa(Fe_{1/2}Ta_{1/2})O_3$; $x = 0.00$, 0.10, 0.25, 0.50, 0.75, 0.90, 1.00 have been carried out. Figure 1 shows the observed, calculated and difference profiles for BNBT–BFT ceramic system after final cycle of refinement. It has been reported that rhombohedral–tetragonal symmetry exists at MPB composition in BNBT [18, 19] and the corresponding X-ray diffraction pattern could be very well fitted in the space group *R*3*c* [22]. Also, the crystal structure of $Ba(Fe_{1/2}Ta_{1/2})O_3$ at room temperature is reported to be rhombohedral of trigonal symmetry [11]. It could be seen that diffraction peaks of $Ba_{0.06}(Na_{1/2}Bi_{1/2})_{0.94}TiO_3$ ($x = 0$) and Ba $(Fe_{1/2}Ta_{1/2})O_3$ ($x = 1$) are consistent with the earlier reports [11, 22] (Fig. 1). Further, it could be observed that the addition of BFT to BNBT matrix, shift in the peak positions and changes in intensities of the peaks (Fig. 2). The crystal structure of $x = 0.10$ was found to be rhombohedral (*R*3*c*) and that with compositions $x \geq 0.25$ the unit cell structure was found to have hexagonal (*P*3*m*1) symmetry. Also, it is evident from Fig. 3 that with the increase in Fe/Ta content in the solid solution, lattice parameters (*a* and *c*) increases in such a way that the ratio *c*/*a*, which is a measure of the tetragonality distortion, remains constant. Also, this can be confirmed from Fig. 3 as the linear fit to the experimental data of *c* and *a* are almost parallel to each other. The shift in diffraction peaks towards lower Bragg's angle also indicated the increase in lattice parameters with increasing *x*. Computer fitting of lattice parameters—concentration (*x*) data yielded the following expressions: $a = 0.2158x + 5.5274$ ($r^2 = 0.9946$) and $c = 13.54154x + 0.53492$ ($r^2 = 0.99163$). Furthermore, it is observed that the value of unit cell volume increases with the increasing $Ba(Fe_{1/2}Ta_{1/2})O_3$ content (Fig. 3), which could be due to the partial replacement of Ti^{4+} (ionic radius: 0.605 Å) with pseudo-cation $(Fe^{3+}_{1/2}Ta^{5+}_{1/2})^{4+}$ having high ionic radii compared to Ti-ion. A second order polynomial fitting to concentration (*x*) dependence of unit cell volume data yielded a relation:

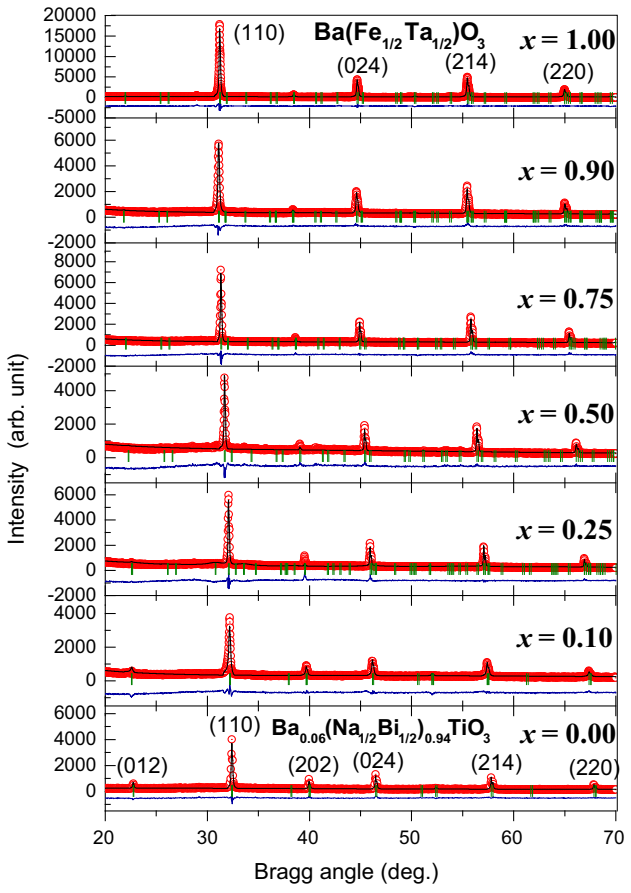

Fig. 1 Rietveld refined XRD patterns of $Ba_{0.06}(Na_{1/2}Bi_{1/2})_{0.94}TiO_3$–$Ba(Fe_{1/2}Ta_{1/2})O_3$ ceramics. *Symbols* represent the observed data points and the *solid lines* their Rietveld fit

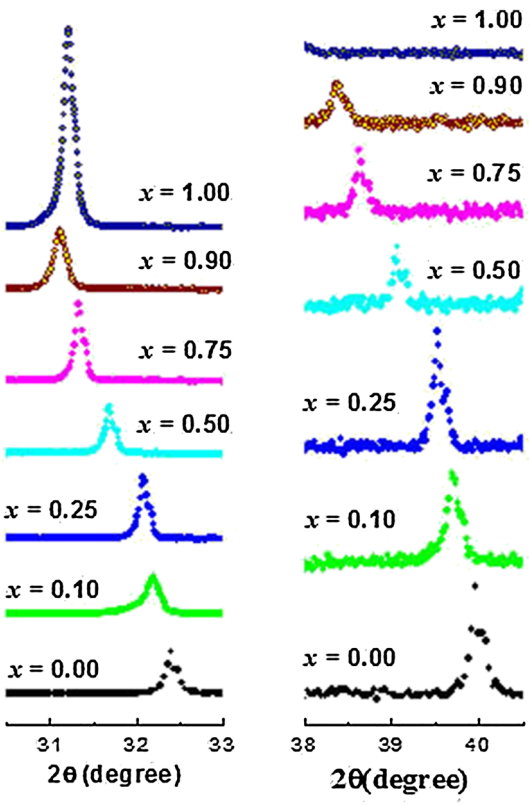

Fig. 2 XRD patterns of selected regions (2θ range 30.5°–33.0° and 38.0°–40.5°) of $Ba_{0.06}(Na_{1/2}Bi_{1/2})_{0.94}TiO_3$–$Ba(Fe_{1/2}Ta_{1/2})O_3$ ceramics

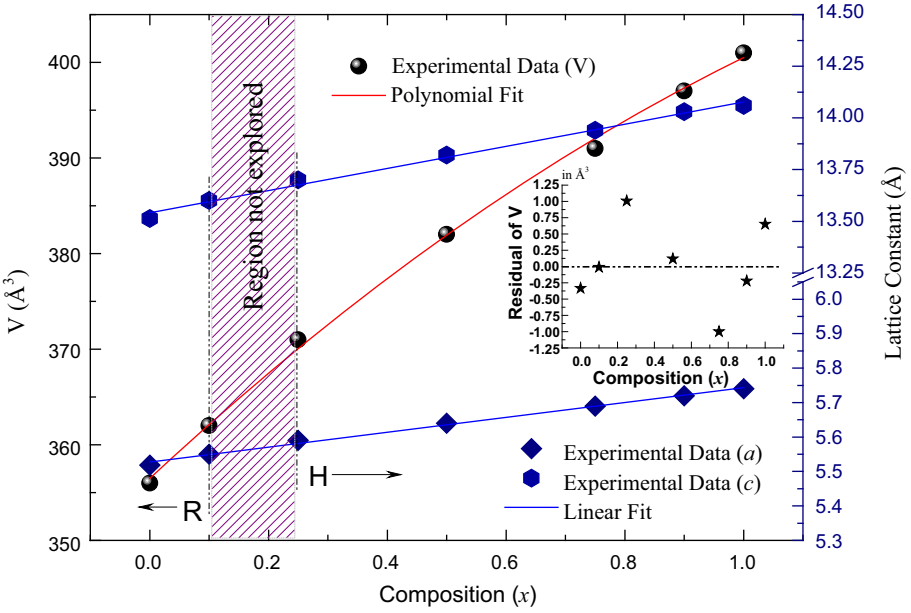

Fig. 3 Compositional dependence of lattice constant (*a*, *c*) and unit cell volume of $Ba_{0.06}(Na_{1/2}Bi_{1/2})_{0.94}TiO_3$–$Ba(Fe_{1/2}Ta_{1/2})O_3$ ceramics. *Inset* residue plot

$V = 356.48571 + 57.71429x - 13.71429x^2$ with $r^2 = 0.9959$. Inset of Fig. 3 shows the residue plot. Furthermore, the XRD results clearly indicated the formation of perovskite type single phase BNBT–BFT solid solutions for the whole range (x).

Figure 4 shows the SEM micrographs of fractured surface of sintered BNBT–BFT ceramics. The nature of the micrographs clearly exhibits the polycrystalline texture and grains are distributed throughout the samples with no and/or very few voids suggesting the high density of the materials. The grains of unequal sizes (1–10 μm) were found for the chosen compositions. Also, the grain size increases with increase in x, attains a maximum at $x = 0.50$ and then decreases with increase in x. The reduction in grain size may be due to the generation of stress which prevent grain boundary movement during the sintering and thus resulted in the reduction of grain sizes [13]. An irregularity in trend occurs for $x = 1.0$ where grain size again shoots up, which is usually termed as an abnormal grain growth or secondary crystallization [23].

Figure 5 shows the EDS spectra of $(1 - x)Ba_{0.06}(Na_{1/2}Bi_{1/2})_{0.94}TiO_3$–$xBa(Fe_{1/2}Ta_{1/2})O_3$ ceramics ($x = 0.00$, 0.50 and 1.00). All the peaks in the patterns have perfectly been assigned to the elements present in $Ba_{0.06}(Na_{0.47}Bi_{0.47})TiO_3$, $Ba_{0.53}Na_{0.235}Bi_{0.235}Fe_{0.25}Ta_{0.25}Ti_{0.50}O_3$ and $Ba(Fe_{0.5}Ta_{0.5})O_3$ ceramics. This clearly indicated the purity and formation of the phase of the ceramics.

Figure 6 shows the IR spectra of the BNBT–BFT ceramics in the mid infrared region. The formation of a perovskite structure can be confirmed by the presence of metal-oxygen band [24]. BNBT consist Ba, Na and Bi at the A-site and Ti at the B-site of the perovskite structure with O at face centre. Reduced masses of Bi–O, Ba–O, Ti–O and Na–O are in decreasing order hence their metal oxide (M–O) bonds have their characteristics wavenumbers in increasing order. Though there could be variations owing to the fact that a particular M–O bond may have degenerate infrared-active vibrations. Considering these aspects, we can infer that in the IR spectra of the BNBT, a spike near 610 cm^{-1} represents the Ti–O stretching mode [25], a strong band at 642 cm^{-1} may be attributed to bonding of either Ba–O or Bi–O and a relatively weak band at 842 cm^{-1} may correspond to Na–O bond. The peak corresponding to Ti–O stretching mode and TiO_6 polyhedron is reported to absorb near 395 cm^{-1} [25] and 410 cm^{-1} and so is not present in the spectrum [26, 27]. Further, with the increment in doping of BFT (x) to BNBT the peak at 642 cm^{-1} becomes narrower, decreases in intensity and shifts towards the lower wavenumber side. The narrowing of the peak may be attributed to increasing number of chemical environments. Specifically, strong absorptive peaks around 587–599 cm^{-1} for $x \geq 0.75$ may be attributed to the Fe–O stretching and bending vibration which is characteristic of octahedral FeO_6 groups in the perovskite compounds [28]. The peaks for $x \geq 0.90$ again go narrow and sharp which may be a confirmation of weak intermolecular interactions is due to decrease in number of chemical environments. The difference in wavenumber of the two dominant (noticeable) peaks decreases throughout the series and seems to coalesce at $x = 1.00$ which seems reasonable because the slight difference in reduced mass of the Ba–O and Fe–O. All the compounds contain weak band at 2800–2900 cm^{-1} which corresponds to carbonate groups, may be due to atmospheric CO_2. The bands at 1639 and 3443 cm^{-1} are assigned to the bending of H–O–H and O–H stretching modes of vibration due to physically

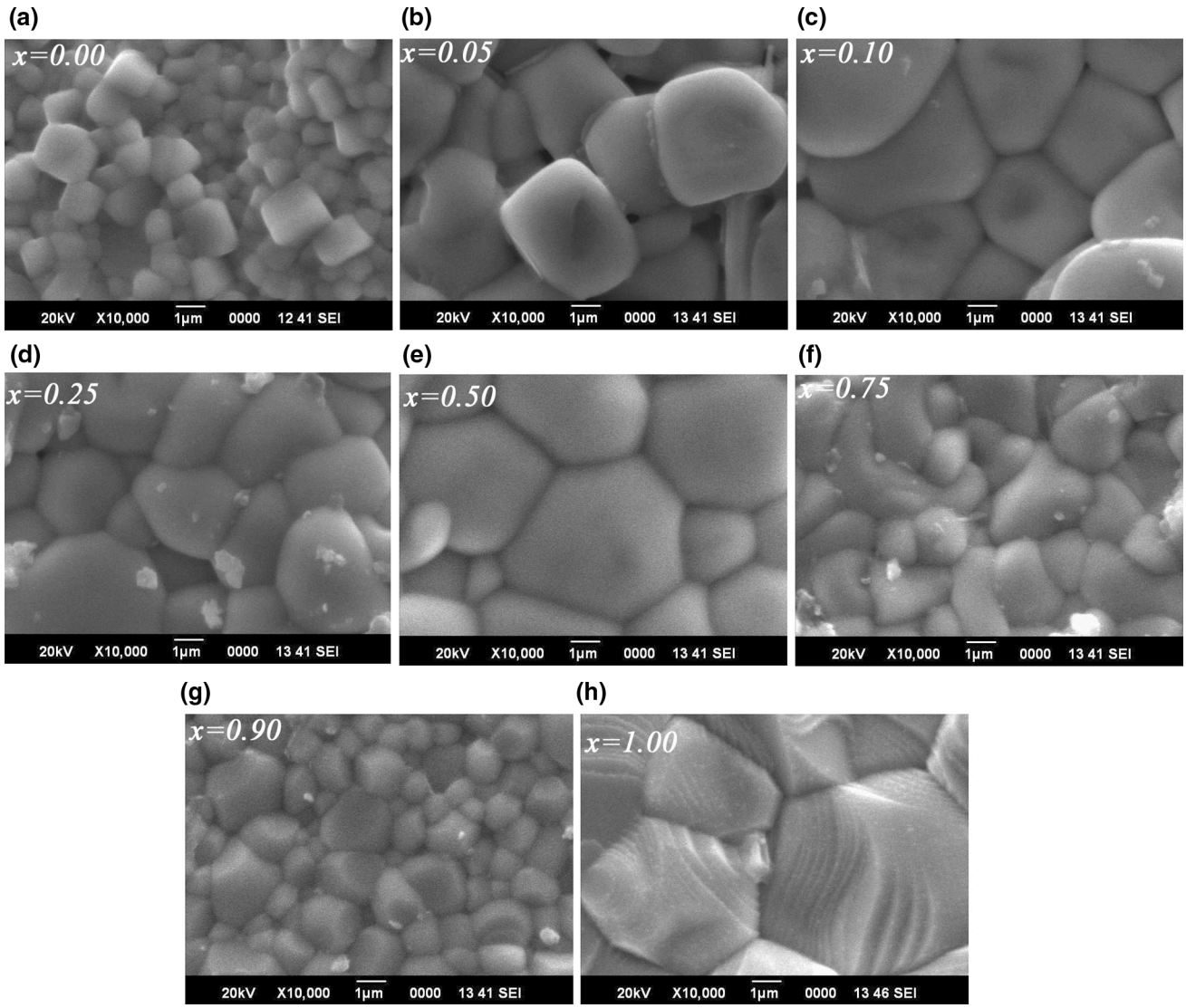

Fig. 4 Scanning electron micrographs of $(1-x)Ba_{0.06}(Na_{1/2}Bi_{1/2})_{0.94}TiO_3$–$xBa(Fe_{1/2}Ta_{1/2})O_3$ ceramics; **a** $x = 0$, **b** $x = 0.05$, **c** $x = 0.10$, **d** $x = 0.25$, **e** $x = 0.50$, **f** $x = 0.75$, **g** $x = 0.90$ and **h** $x = 1.0$

adsorbed water molecules on the surface of the sample during palletisation with KBr for the entire series of BNBT–BFT ceramic system.

Figure 7a, b, respectively, show the first-order Raman spectra of $Ba_{0.06}(Na_{0.47}Bi_{0.47})TiO_3$ and $Ba(Fe_{0.5}Ta_{0.5})O_3$. The peaks of BNBT were found to be Gaussian in line-shape contrary to the expected Lorentzian line-shape fitting [29] over the exponential background from Rayleigh tail. The Peaks (FWHM in parenthesis) were observed at 133.3 (19.2), 281.3 (53.4), 536.2 (49.7), 615.3 (28.11) and at 799.4 (79.2) cm^{-1}. The Gaussian peak profile observed in the Raman spectra arises due to particle size distribution in the sample [29]. Contrary to the BNBT, BFT shows intense sharp and multiple Lorentzian peaks. As shown in Fig. 7c, no new peaks are observed with increasing BFT content (x), indicating thereby the formation of solid solutions of BNBT–BFT and consequently the absence of formation of any new phase. Besides, it can be seen from Fig. 7c that the bands with lower intensities appear at frequencies that do not differ much from those of the pure BFT. Since the Raman spectra of BNBT and BFT differ much, the evolution of the structural changes of BNBT–BFT solid solutions, which depend on composition, can be followed using XRD and dielectric data. Also, the Raman bands are quite broad, which in fact is associated with the disorder of cations at the coordinated sites, and to some overlapping Raman modes [30].

The temperature variation of dielectric constant (ε) and loss tangent (tanδ) for BNBT–BFT ceramics at 1 and 10 kHz are, respectively, given in Figs. 8 and 9. All the plots in Fig. 8 find a maximum (T_m). Also, the phase transition in BNBT is found to be fairly sharp and as the

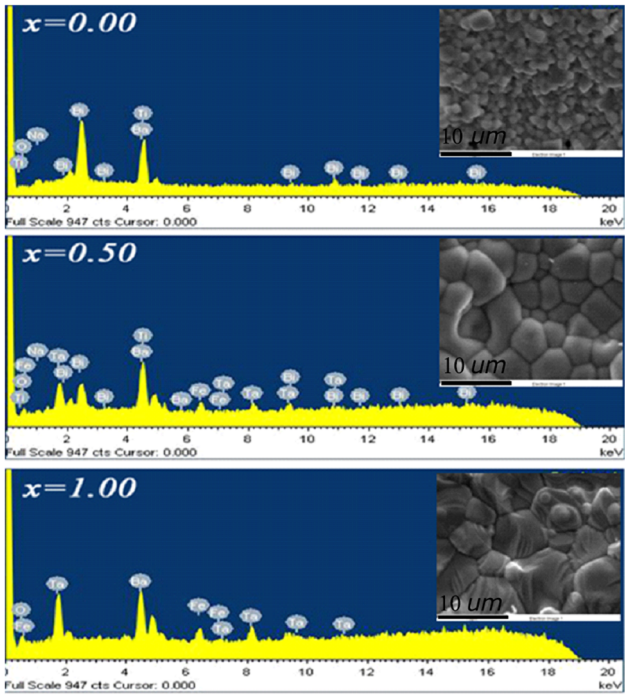

Fig. 5 EDX patterns of $(1 - x)Ba_{0.06}(Na_{1/2}Bi_{1/2})_{0.94}TiO_3$–$xBa(Fe_{1/2}Ta_{1/2})O_3$; $x = 0$, 0.5 and 1.0 ceramics

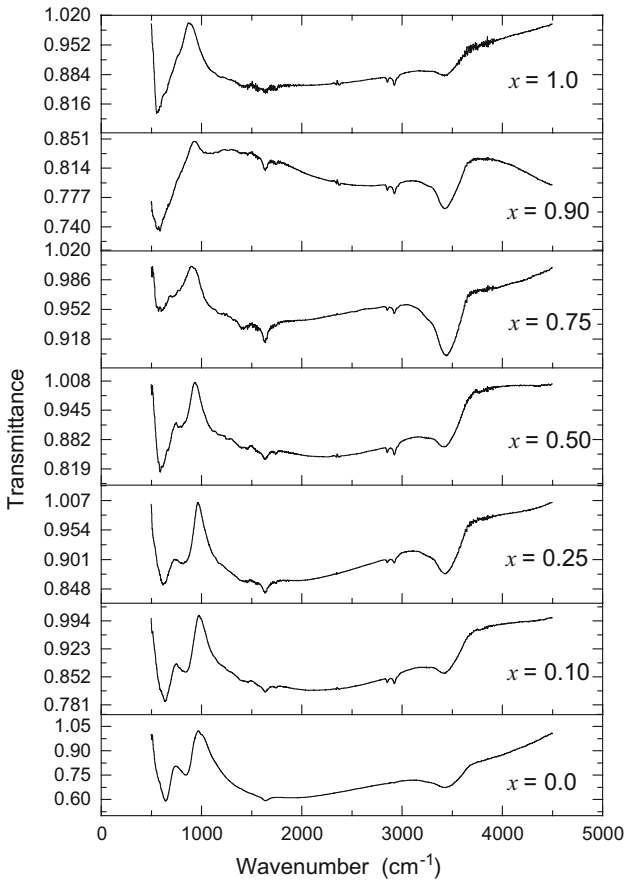

Fig. 6 FTIR spectra of $(1 - x)Ba_{0.06}(Na_{1/2}Bi_{1/2})_{0.94}TiO_3$–$xBa(Fe_{1/2}Ta_{1/2})O_3$ ceramics

BFT-content increases in BNBT matrix the phase transition becomes diffuser. The broadening of ferroelectric phase transition in solid solutions, in which identical crystallographic sites are randomly occupied by different types of ions, is attributed to composition fluctuations. It is known that broadening of phase transition with composition fluctuation takes place only when the long range cooperative interactions between ions are weak enough. When the long range cooperative forces are weak, the local field acting on a lattice site is produced by the small number of ions around the site that is ions contained in the spherical region within which the interaction exist with the lattice point at the center. Under such a condition the fluctuations (local) in composition have a great influence on the broadening of phase transition. Thus substitution of Fe^{3+} or Ta^{5+} ions for Ti^{4+} into the B-site of BNBT matrix seems to weakens the long range cooperative forces between the B-site ions, causing the composition fluctuation effective for the phase transition broadening. Thus diffuse ferroelectric phase transition for $0.25 \leq x \leq 0.75$ could be due to the convergence of a great number of local ferroelectric phase transitions, which are caused by fluctuations in the local composition [31]. In addition to the effects on short range forces, a direct long range interaction between ions can originate from the local permanent electric dipoles with random orientations due to the ion pairs (Fe^{3+}, Ti^{4+}), (Fe^{3+}, Ta^{5+}), (Ti^{4+}, Ta^{5+}), etc. arranged together in the neighbouring B-positions [31]. This causes an additive direct disturbance of the long range cooperative interactions in crystals which may be responsible for a rapid phase transition broadening with increase in BFT-content. This is also responsible for non-linear and steady decrement of Curie temperature with BFT-content. When BFT-content is excess of 75% the broadening in phase transition reduces owing to strengthening of long range cooperative forces.

Figure 10 illustrates the variation of T_m, tan δ at room temperature and dielectric constant at room temperature (ε_{RT}) and at T_m (ε_{max}) with increasing BFT-content (x). It is observed that the value of ε_{RT} (=3.47 × 10^4) and $\tan\delta_{RT}$ (=2.107) are found, respectively, to be maximum for the composition with $x = 0.75$ and 0.50 while the maximum value of ε_{max} (=3.22 × 10^6) is observed in case of $x = 0.50$. The rise in dielectric constant with BFT-content may be attributed to various factors. The interaction of local permanent electric dipoles viz. (Fe^{3+}, Ti^{4+}), (Fe^{3+}, Ta^{5+}), (Ti^{4+}, Ta^{5+}), etc. with random orientations is weak due to the phonon mode softening and structural relaxation in these regions so the dipoles get easily polarized under external alternative electric field, enhancing the dielectric responses [31]. Thus domain wall vibration is one contribution component to the dielectric constant (which is called

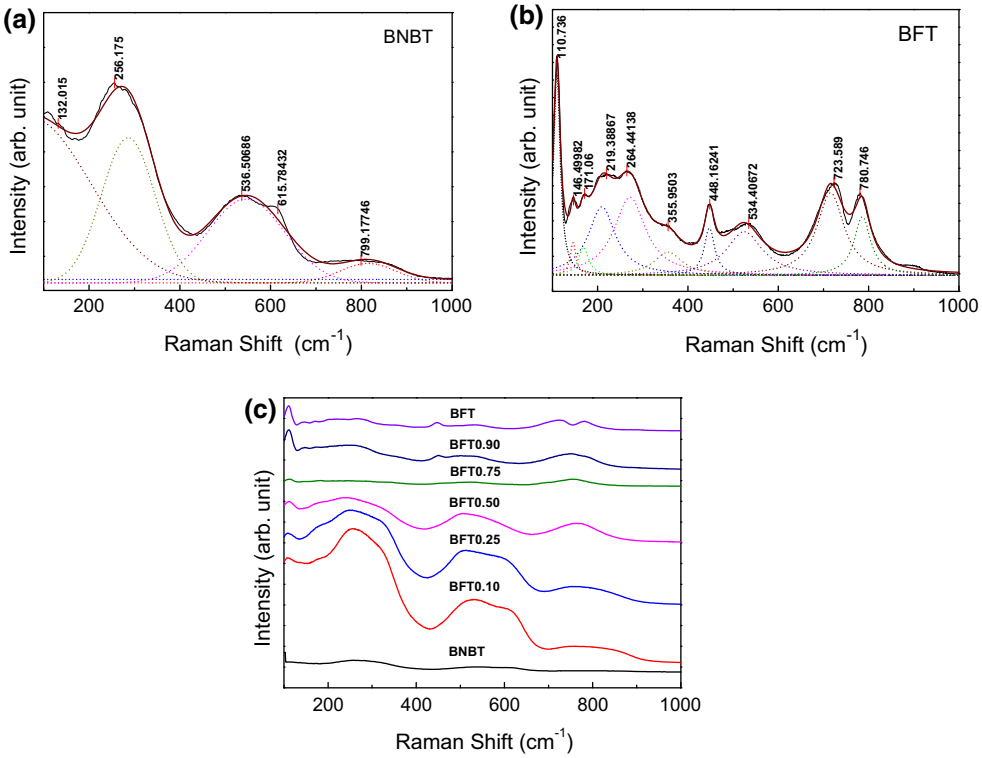

Fig. 7 **a** Raman spectra of $Ba_{0.06}(Na_{1/2}Bi_{1/2})_{0.94}TiO_3$ and fitted peaks with Gaussian components, **b** Raman spectra of $Ba(Fe_{1/2}Ta_{1/2})O_3$ and deconvoluted with Lorentzian components and **c** changes in the Raman spectra with increasing $Ba(Fe_{1/2}Ta_{1/2})O_3$ doping (x) in $Ba_{0.06}(Na_{1/2}Bi_{1/2})_{0.94}TiO_3$ matrix

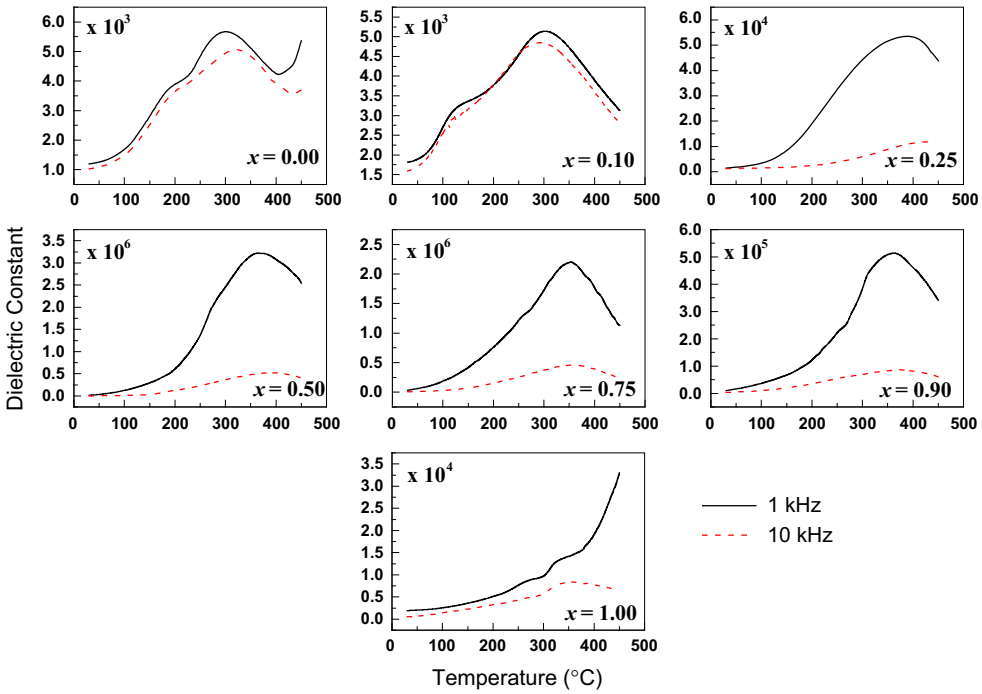

Fig. 8 Temperature dependence of dielectric constant of $Ba_{0.06}(Na_{1/2}Bi_{1/2})_{0.94}TiO_3$–$Ba(Fe_{1/2}Ta_{1/2})O_3$ ceramics at 1 and 10 kHz

orientational polarization). The other contributing component is ionic polarization. If some of the Ta^{5+} ions substitutes Ti^{4+} ions, cation vacancies may be created to maintain charge neutrality [32]. This may be due to the fact that the cation vacancies allow ionic motion in the direction of the applied electric field and consequently increasing the concentration of charge at the interfaces. Thus the sample gets ionically polarized and such ionic movements produces a counter field opposite to the externally applied field [33]. Thereby the effective field inside the sample decreases, which lead to increase in the dielectric constant. As $x \geq 0.75$ the dielectric response

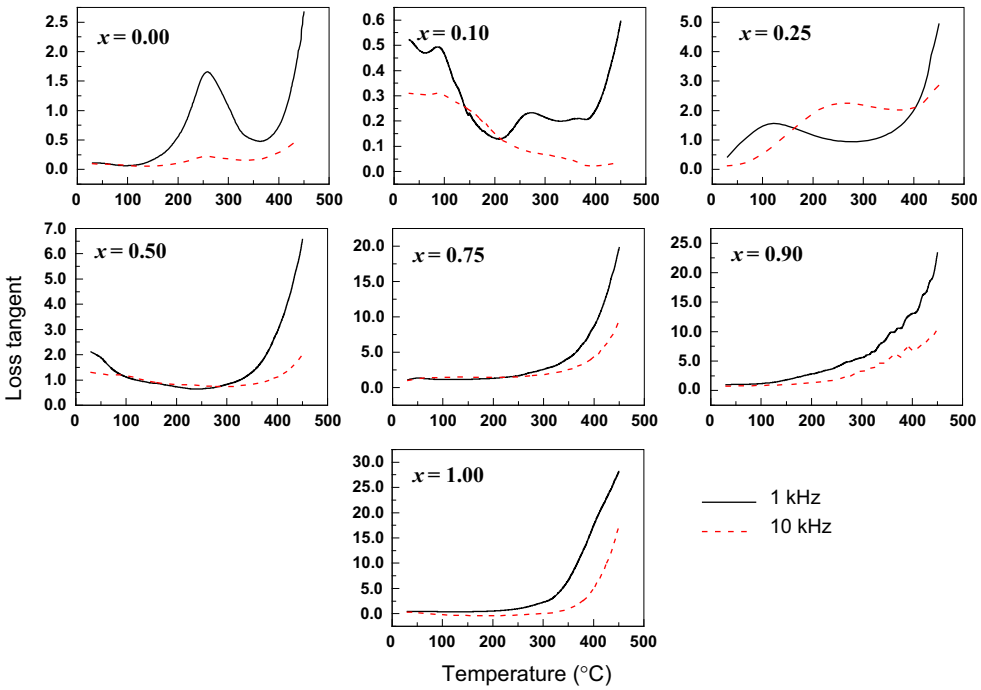

Fig. 9 Temperature dependence of loss tangent of $Ba_{0.06}(Na_{1/2}Bi_{1/2})_{0.94}TiO_3$–$Ba(Fe_{1/2}Ta_{1/2})O_3$ ceramics at 1 and 10 kHz

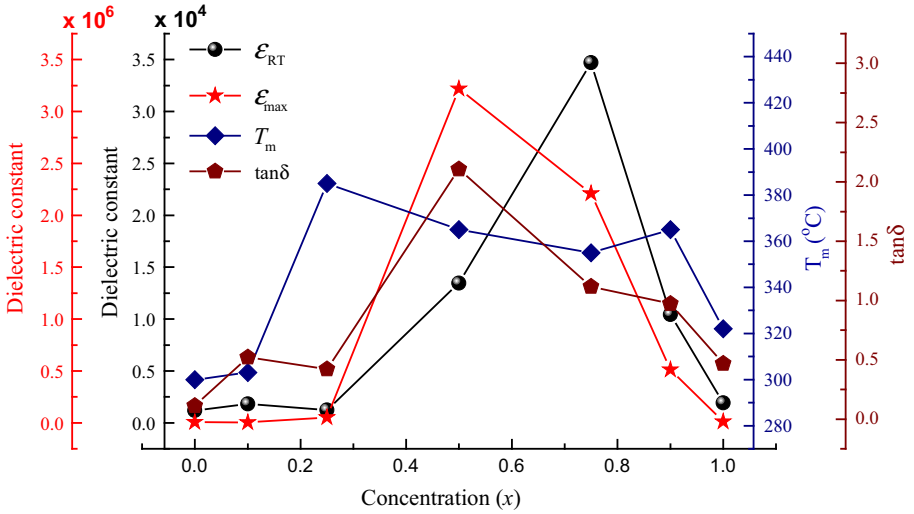

Fig. 10 Compositional dependence of dielectric parameters of $Ba_{0.06}(Na_{1/2}Bi_{1/2})_{0.94}TiO_3$–$Ba(Fe_{1/2}Ta_{1/2})O_3$ ceramics at 1 kHz

again decreases as the interaction between the local dipoles increase and the strong local interaction randomizes the permanent electric dipoles, thus reducing the average polarization of the samples. Furthermore, grain boundary is thought to have a lower dielectric constant than the ferroelectric grain, so with increasing grain size, the fraction of grain boundary volume decreases and the corresponding ceramics dielectric constant increases. In the present case, both grain size as well as dielectric constant are found to be maximum for $x = 0.50$ which supports this fact. A similar kind of increment in dielectric constant due to increase in grain size was explained by Lin et al. [34] by modifying Ginsburg–Landau–Devonshire thermodynamic theory.

4 Summary

Perovskite type lead-free ceramics, $(1 - x)Ba_{0.06}(Na_{1/2}Bi_{1/2})_{0.94}TiO_3$–$xBa(Fe_{1/2}Ta_{1/2})O_3$ $(0 \leq x \leq 1.0)$ were synthesized using the solid state reaction method. X-ray diffraction studies of all the ceramics suggested the formation of a single phase with crystal structure transforming from rhombohedral–tetragonal ($R3c$) to orthorhombic ($P3m1$) symmetry with the increase in $Ba(Fe_{1/2}Ta_{1/2})O_3$ content. Raman and FTIR spectra also confirmed the formation of solid solution without any new phase. The dielectric constant as a function of temperature showed the giant permittivity $\sim 10^6$ in

$x = 0.50$ and 0.75 compositions and the phase transition was found to be of diffusive character. The simultaneous occurrence of compositional fluctuations and weak ferroelectric interactions were considered to be the main cause for diffusivity.

References

1. Z. Wang, X.M. Chen, L. Ni, Y.Y. Liu, X.Q. Liu, Appl. Phys. Lett. **90**, 102905 (2007)
2. I.P. Raevski, S.A. Prosandeev, A.S. Bogatin, M.A. Malitskaya, L. Jastrabik, J. Appl. Phys. **93**, 4130 (2003)
3. C.-Y. Chung, Y.H. Chang, G.J. Chen, J. Appl. Phys. **96**, 6624 (2004)
4. C.C. Homes, T. Vogt, S.M. Shapiro, S. Wakimoto, A.P. Ramirez, Science **293**, 673 (2001)
5. S. Bhagat, K. Prasad, Phys. Status Solidi A **207**, 1232 (2010)
6. F. Galasso, L. Katz, R. Ward, J. Am. Chem. Soc. **81**, 820 (1959)
7. W.H. Jung, J.H. Lee, J.H. Sohn, H.D. Nam, S.H. Cho, Mater. Lett. **56**, 334 (2002)
8. A.I. Agranovskaya, Bull. Acad. Sci. USSR Phys. Ser. **24**, 1271 (1960)
9. V.S. Filip'ev, E.G. Fesenko, Sov. Phys. Crystallogr. **6**, 616 (1961)
10. F. Galasso, W. Darby, J. Phys. Chem. **66**, 131 (1962)
11. G. Li, S. Liu, F. Liao, S. Tian, X. Jing, J. Lin, Y. Uesu, K. Kohn, K. Saitoh, M. Terauchi, N. Di, Z. Cheng, J. Solid State Chem. **177**, 1695 (2004)
12. Z. Wang, X.M. Chen, X.Q. Liu, J. Appl. Phys. **105**, 034114 (2009)
13. T. Phatungthane, G. Rujijanagul, K. Pengpat, S. Eitssayeam, T. Tunkasiri, L.F. Cotica, R. Guo, A.S. Bhalla, Curr. Appl. Phys. **14**, 1819 (2014)
14. C. Li, Z. Zang, W. Chen, Z. Hu, X. Tang, W. Hu, K. Sun, X. Liu, W. Chen, Opt. Express **24**, 15071 (2016)
15. G. Li, F.W.R. Rivarola, N.J.L.K. Davis, S. Bai, T.C. Jellicoe, F. de la Peña, S. Hou, C. Ducati, F. Gao, R.H. Friend, N.C. Greenham, Z.-K. Tan, Adv. Mater. **28**, 3528 (2016)
16. J. Rödel, W. Jo, K.T.P. Seifert, E.-M. Anton, T. Granzow, J. Am. Ceram. Soc. **92**, 1153 (2009)
17. B.-J. Chu, D.-R. Chen, G.-R. Li, Q.-R. Yin, J. Eur. Ceram. Soc. **22**, 2115 (2002)
18. T. Takenaka, H. Nagata, J. Eur. Ceram. Soc. **25**, 2693 (2005)
19. T. Takenaka, K. Maruyama, K. Sakata, Jpn. J. Appl. Phys. Part 1 **30**, 2236 (1991)
20. R.D. Shanon, Acta Crystallogr. A **32**, 751 (1976)
21. V. Sivasubramanian, V.R.K. Murthy, B. Viswanathan, Jpn. J. Appl. Phys. **36**, 194 (1997)
22. R. Ranjan, A. Dviwedi, Solid State Commun. **135**, 394 (2005)
23. K. AmarNath, K. Prasad, Adv. Mater. Res. **1**, 115 (2012)
24. D. Lee, M.G. Kim, S. Ryu, H.M. Jang, S.G. Lee, Appl. Phys. Lett. **86**, 222903 (2005)
25. J.T. Last, Phys. Rev. **105**, 1740 (1957)
26. K.K.P. Srivastava, K.K. Sinha, D. Banerjee, S. Ghosh, Indian J. Pure Appl. Phys. **41**, 393 (2003)
27. C.H. Perry, B.N. Khanna, Phys. Rev. A **2**, 135 (1964)
28. S.K. Sahoo, K. Agarwal, A.K. Singh, B.G. Polke, K.C. Raha, Int. J. Eng. Sci. Techol. **2**, 118 (2010)
29. S.K. Roy, S. Chaudhuri, R.K. Kotnala, D.K. Singh, B.P. Singh, S.N. Singh, K.P. Chandra, K. Prasad, Mater. Sci. Pol. **34**, 437 (2016)
30. F. Bahri, H. Khemakhem, M. Gargouri, A. Simon, R. von der Mühll, J. Ravez, Solid State Sci. **5**, 1229 (2003)
31. V.A. Isupov, Ferroelectrics **143**, 109 (1993)
32. L. Dong, D.S. Stone, R.S. Lakes, J. Appl. Phys. **111**, 084107 (2012)
33. S. Meloni, T. Moehl, W. Tress, M. Franckevičius, M. Saliba, Y.H. Lee, P. Gao, M.K. Nazeeruddin, S.M. Zakeeruddin, U. Rothlisberger, M. Graetzel, Nat. Commun. **7**, 10334 (2016)
34. S. Lin, T. Lü, C. Jin, X. Wang, Phys. Rev. B **74**, 134115 (2006)